Check for updates

Aggregation-induced emission enhancement (AIEE)-active boron-difluoride dyes with reversible mechanochromic fluorescence†

Xiaojing Yan,[a] Pengcheng Zhu,[a] Zhiguo Zhou, [ID][b] Hong Yang,[b] Haichuang Lan[a] and Shuzhang Xiao [ID] *[a]

A novel class of solid-emissive boron-difluoride derivatives, using phenanthrenequinone hydrazone as ligands, were designed and efficiently synthesized. These dyes exhibit weak fluorescence in dilute solutions, but much higher fluorescence efficiency in aggregate states with a large stokes shift (over 70 nm) due to the their aggregation-induced emission enhancement (AIEE) characteristics. According to their photophysical properties and X-ray single crystal structure analysis, the AIEE was ascribed to the H(J)-aggregate formation aided by multiple intermolecular interactions to restrict intramolecular motion in the solid state. Moreover, their solid emissions could be reversibly tuned between "on" and "off" by mechanical grinding and recrystallization, due to the stacking model transition between H(J)-aggregation with loose molecular packing and J-aggregation with intense intermolecular interactions.

1 Introduction

Fluorescent dyes have been receiving continuous attention for their potential applications in advanced science and technology. Although large number of highly fluorescent chromophores have been developed during the past decades, boron-difluoride dyes are still of great interest due to their numerous advantages, such as high fluorescence intensity, excellent chemical- and photochemical-stability, long excited-state lifetime and narrow emission spectra.[1] However, typical boron-difluoride dyes (BODIPY, namely 4-bora-4,4-difluoro-pyrromethene) exhibit highly planar chemical structures, which would facilitate the formation of π–π stacking and lead to aggregate-induced fluorescence quenching. Moreover, the high symmetry character of BODIPYs makes the potential energy surfaces of the ground and excited state less distinct.[2–4] Therefore, BODIPY dyes possess small stokes shift and are usually non-emissive in the solid state.

For the purpose of practical applications in photoelectric devices, it's quite important to maintain their emissions in the solid state and increase their Stokes shifts. Up to now, there have been a few techniques to construct solid-emissive boron-

difluoride complexes, such as introducing bulky groups around the BF₂ chelate to alleviate the intermolecular π–π stacking by steric effect and designing intermolecular non-covalent bonding to promote non-parallel packing.[5] During the recent years, we have adopted the second technique to develop a series of boron-difluoride dyes based on the ligand of 2-(2′-pyridyl) imidazole derivatives, and found that these boron-difluoride dyes (BOPIM) exhibit quite large stokes shift (over 100 nm) and high fluorescence intensity in the solid state.[6–11] It seems that low-symmetrization of the structures is quite effective to cause more energetically distinguished ground and excited states to enlarge the Stokes shift.[12] However, the synthesis of BOPIM dyes is tedious because of the low synthetic yields. On the other hand, the chemical stability of BOPIM dyes needs to be enhanced because they tend to decompose under basic conditions.

During the recent years, limited number of solid-emissive boron-difluoride dyes with aggregation-induced emission enhancement (AIEE) have been reported. AIEE substances were first developed by Tang *et al.* in 2001, which emits weak fluorescence when dissolved, but strong luminescence in the aggregate state.[13] Fluorescent dyes with AIEE properties have many advantages for practical application in the fields of analytical detection, fluorescence imaging and luminescent devices. For AIEE-active boron-difluoride dyes, non-pyrrole-based ligands with asymmetrical structures were normally adopted, such as β-diketone or *N*-substituted β-diketone derivatives,[14–18] β-iminoenolate derivatives[19–27] and others.[28–35] All these dyes bear rotatable bulky aromatic groups, which promotes the non-irradiative decay in dilute solutions. But in the solid state, the rotation was restricted, therefore, they

[a]College of Biological and Pharmaceutical Sciences, China Three Gorges University, Yichang 443002, Hubei, P. R. China. E-mail: shuzhangxiao@ctgu.edu.cn; Fax: +86 717 6397478

[b]The Education Ministry Key Lab of Resource Chemistry, Shanghai Normal University, Shanghai 200234, China

† Electronic supplementary information (ESI) available: Additional photophysical data, figures and table, crystal structure analysis. CCDC 1946768. For ESI and crystallographic data in CIF or other electronic format see DOI: 10.1039/c9ra07437f

emit low or no fluorescence in dilute solutions but intense fluorescence in the solid state. Although a few examples of AIEE complexes ascribed to J aggregation,[36,37] excimer formation[38–40] have been reported, there have been limited reports on AIEE boron-difluoride dyes based on J(H)-aggregate which are formed between chromophores with tight chromophore spacing and strong coupling,[41] and it is still highly significant to explore new AIEE dyes based on boron-difluoride chromophore for developing new functional luminescent materials. On the other hand, the aggregation and deaggregation might be manipulated by external stimuli (heat, pressure and *etc.*) to provide environment-sensitive materials. Herein, we designed and synthesized two novel boron-fluoride derivatives with AIEE properties and investigated their mechanochromic properties.

2 Experimental

2.1 Materials and methods

All starting materials were obtained from commercial supplies and used as received. ^{1}H NMR spectrum was recorded on Bruker 400 NMR instruments, using CDCl$_3$ as solvent. PXRD diagrams were tested on a D8 ADVANCE (Bruker). UV-vis and fluorescent measurements were carried out on Shimadzu UV-2600 and Hitachi F-4600, respectively. The fluorescence quantum yields in solutions are calculated using rhodamine B as a reference, and the fluorescence quantum yields of the solid powders were measured from a Hamamatsu Absolute PL Quantum Yield Spectrometer C11347. Size distribution were measured on a Malvern Zetasizer (Nano ZS90). Single crystal of **PHPO-BF$_2$** suitable for X-ray diffraction measurements was obtained by slow evaporation from a mixture of dichloromethane and petroleum ether. X-ray diffraction data were collected on a BRUKER D8 QUEST diffractometer. And the CCDC number is 1946768.† The initial powder samples for mechanochromism study are obtained by vacuum evaporation of column eluents, and ground samples were obtained by grinding in a mortar manually.

Geometry optimization were performed by density functional theory (DFT) at B3LYP with the 6-31+G(d,p) basis sets.[42] The search for potential crystal structures was performed by Accelrys Polymorph Predictor module of the Materials Studio software, using the simulated annealing algorithm of Karfunkel and Gdanitz.[43] The molecular cluster with intense intermolecular π–π interactions in single crystal was chosen as input and calculated at the M06-2X/6-31+G(d,p) level with dispersion correction (empirical dispersion = GD3).[44] Then intermolecular interactions were analyzed by Multiwfn and visualized by VMD.[45] The intermolecular interactions were shown as green clouds.

2.2 Synthesis

Precursors in Scheme 1 were prepared according to literature procedure.[46] The precursors (6.7 mmol) and triethylamine (48.3 mmol, 6.7 mL) were dissolved in anhydrous dichloromethane (30.0 mL) and stirred at ice bath for 10 min under an

atmosphere of argon. Then boron trifluoride etherate (73.8 mmol, 9.1 mL) was added, and the resultant mixture was stirred at room temperature overnight. After the reaction was quenched with water and then extracted by dichloromethane, the organic phase was dried over anhydrous sodium sulfate and then evaporated under vacuum. The obtained crude product was purified by recrystallization from a mixture of dichloromethane and petroleum ether to afford red solids (yield: 95% for **PHPO-BF$_2$**; 90% for **NHPO-BF$_2$**).

PHPO-BF$_2$. ^{1}H NMR (400 MHz, CDCl$_3$) δ 8.77 (d, J = 8.1 Hz, 1H), 8.71 (d, J = 7.9 Hz, 1H), 8.61 (d, J = 8.3 Hz, 1H), 8.55 (d, J = 7.9 Hz, 1H), 8.16 (d, J = 7.8 Hz, 2H), 7.95 (t, J = 7.7 Hz, 1H), 7.79–7.66 (m, 3H), 7.66–7.54 (m, 3H). ^{13}C NMR (101 MHz, CDCl$_3$) δ 152.54, 145.16, 137.08, 134.06, 130.45, 129.44, 129.09, 128.92, 128.03, 127.86, 127.12, 126.62, 124.41, 123.23, 122.97, 122.74, 122.09. HRMS: calcd for C$_{20}$H$_{13}$BF$_2$N$_2$O [M + H]$^{+}$ 347.1176, found 347.1165.

NHPO-BF$_2$. ^{1}H NMR (400 MHz, CDCl$_3$) δ 8.78 (m, 2H), 8.72 (s, 1H), 8.62 (d, J = 8.3 Hz, 1H), 8.56 (d, J = 8.0 Hz, 1H), 8.27 (dd, J = 9.0, 2.0 Hz, 1H), 8.12–8.01 (m, 2H), 7.95 (m, 2H), 7.83–7.67 (m, 3H), 7.67–7.58 (m, 2H). ^{13}C NMR (101 MHz, CDCl$_3$) δ 152.28, 142.65, 137.10, 134.22, 134.09, 133.86, 133.12, 129.66, 129.60, 129.17, 129.01, 128.07, 127.93, 127.89, 127.31, 127.22, 126.75, 124.50, 123.32, 123.21, 123.07, 122.23, 119.36. HRMS: calcd for C$_{24}$H$_{15}$BF$_2$N$_2$O [M + H]$^{+}$ 397.1342, found 397.1323.

3 Results and discussion

The photophysical properties of **PHPO-BF$_2$** and **NHPO-BF$_2$** were studied in various organic solvents with different polarity. The absorption band of **PHPO-BF$_2$** was centred at 480 nm in THF, but shifts to 496 nm in chloroform (Fig. 1A). Its absorptions in hexane and acetonitrile were found at 490 and 491 nm, respectively. For **NHPO-BF$_2$** (Fig. 1C), the maximum absorption bands were found at 505, 514, 496, 510 nm in hexane, chloroform, THF and acetonitrile, respectively. It seems that the absorption of the two boron-difluoride dyes was non-dependent on the polarity of the solvent, indicating that intramolecular charge transfer (ICT) should be not significant for these two compounds. This speculation is accordance to the result of density functional theory (DFT) calculation (Fig. S1†). For both boron-difluoride dyes, the HOMO and LUMO distributions were donated by all atomic orbitals in the whole π system, and there was only slight difference between the HOMO and LUMO orbitals.
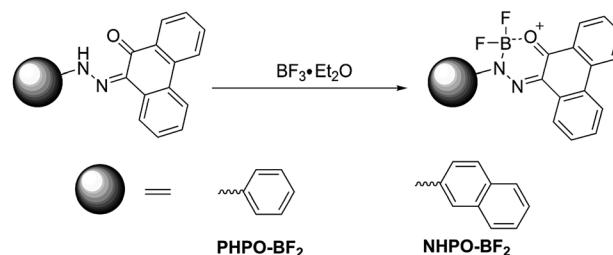
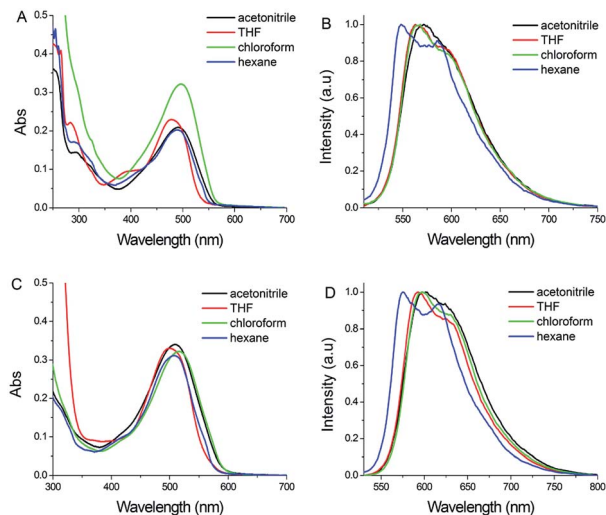Scheme 1 Synthesis of PHPO-BF$_2$ and NHPO-BF$_2$.

Fig. 1 (A) Absorption and (B) fluorescence spectra of PHPO-BF$_2$ in different solvents; (C) absorption and (D) fluorescence spectra of NHPO-BF$_2$ in different solvents (1.0×10^{-5} M).

Fluorescence spectra of **PHPO-BF$_2$** showed two emissive bands in hexane, centred at 546 and 586 nm, respectively (Fig. 1B). Concentration-dependent fluorescence in hexane indicates that there was only one main emissive peak (551 nm) in highly dilute hexane solution (Fig. S2†). With concentration increasing, the emission around 580 nm appeared. Considering the planar structure of the phenanthrene unit in the boron-difluoride dye, significant intermolecular π–π interactions might be present to induce the fluorescence red-shift, and J or H aggregates might be formed in concentrated hexane solutions. Solvent polarity usually affects the fluorescence of D–π–A dyes significantly, but no obvious fluorescence difference was found in solvents with different polarity, due to the inapparent ICT character of these two dyes (Fig. 1B and D).

Concentration-dependent absorption and fluorescence in THF was also measured to investigate the evolution of molecular assembly of these two dyes, which can provide more information about aggregation. The fluorescence of **PHPO-BF$_2$** in dilute THF solution (1.0×10^{-7} M) is centred at 613 nm. When the concentration increases to 1.0×10^{-5} M, the fluorescence blue-shifts to 566 nm. If its concentration further increases, red-shift of the emission was observed (Fig. S3†). It seems that **PHPO-BF$_2$** tends to form H-aggregate first in concentrated THF solution ($C < 5.0 \times 10^{-4}$ M), which is also supported by concentration-dependent absorption spectra (Fig. S3A†). In dilute solution, there appears broad absorption band ranging from 500–700 nm, and this broad absorption band disappears in concentrated solution. But in highly concentrated THF solution ($C > 5.0 \times 10^{-4}$ M), different stacking modes might coexist to form both H-aggregate and J-aggregate, resulting in red-shift of the fluorescence.

For **NHPO-BF$_2$**, it emits at 612 nm in dilute THF solution (1.0×10^{-7} M), and it blue-shifts to 590 nm when the concentration increases to 1.0×10^{-5} M (Fig. S4†). Similar as **PHPO-BF$_2$**, significant red-shift was observed with concentration further

increasing. It seems that **NHPO-BF$_2$** tends to form H-aggregate when the concentration is between 1.0×10^{-7} M and 1.0×10^{-4} M, and then J-aggregate in more concentrated solutions. The slight different molecular assembly behavior could be ascribed to the different π system of phenyl unit and naphthyl group.

Most boron-difluoride compounds (such as BODIPY dyes) are highly fluorescent in dilute solutions, but prone to fluorescence quenching in the solid state due to intermolecular π–π interactions.[5] However, for the two boron-difluoride compounds, their fluorescences were very weak in dilute solutions (Table S1†), and their quantum yields were less than 0.1% in all the solvents studied (except in chloroform), possibly due to the non-irradiative decay via energy lost from the rotation of the aromatic rings (phenyl and naphthyl ring). In fact, their emissions in dilute solutions can hardly be observed by naked eyes. However, the solid powders of these two boron-difluoride compounds emit much stronger fluorescences and these emissions could be visible observed by a portable UV lamp. Since these two compounds emit stronger fluorescence in the solid state than in dilute solutions, we suppose they may exhibit AIEE characteristics.

The AIEE properties of two boron-difluorides were tested by absorption and fluorescence spectroscopy in a binary solvent system containing THF and water. Considering the hydrophobicity of boron-difluoride dyes, these luminogens should be able to precipitate in the aqueous mixtures with high water fractions (f_w), which was proved by the fact that these two compound exhibited Tyndall effect in mixed solutions containing large amount of water (Fig. S5†). As shown in Fig. 2B, as the water content (f_w) is from 0% to 10%, the fluorescence intensity becomes weakened for **PHPO-BF$_2$**, possible due to the intermolecular interaction between water and the dye. With f_w between 10% and 70%, the fluorescence intensity is gradually increased, and reached a maximum at f_w 80% ($\Phi_f = 0.6\%$). With water amount further increasing, the fluorescence weakened again with a significant red shift. **PHPO-BF$_2$** emits at 566 nm in dilute THF solution, but its fluorescence shifts to 660 nm when f_w reaches 99% ($\Phi_f = 0.2\%$). It's clear that emissive aggregate of **PHPO-BF$_2$** has been formed at f_w 80%, and it shows more intense fluorescence than in dilute THF solution due to the restriction of rotation to alleviate the radiationless relaxation channel.

To investigate the fluorescence quenching in THF/H$_2$O containing large amount of water, particle size measurement for these samples was performed (Fig. S6†). The size distribution of **PHPO-BF$_2$** in the solution containing 80% water is in a normal fashion with average size around 440 nm. But for the sample containing 99% water, a much wider size distribution was observed, implying that it might agglomerate to form amorphous aggregate. The formation of amorphous aggregate should be responsible for the decreased fluorescence intensity. On the other hand, the red-shift of the fluorescence in THF/H$_2$O containing large amount of water might be aroused by the formation of J-aggregate. The absorption measurement also supports this hypothesis, because a shoulder band around 570 nm appeared (Fig. 2A).

For **NHPO-BF$_2$**, there is no significant fluorescence change with f_w between 0% to 60%. However, the fluorescence intensity gets greatly enhanced when f_w is beyond 70% ($\Phi_f = 1.3\%$), and
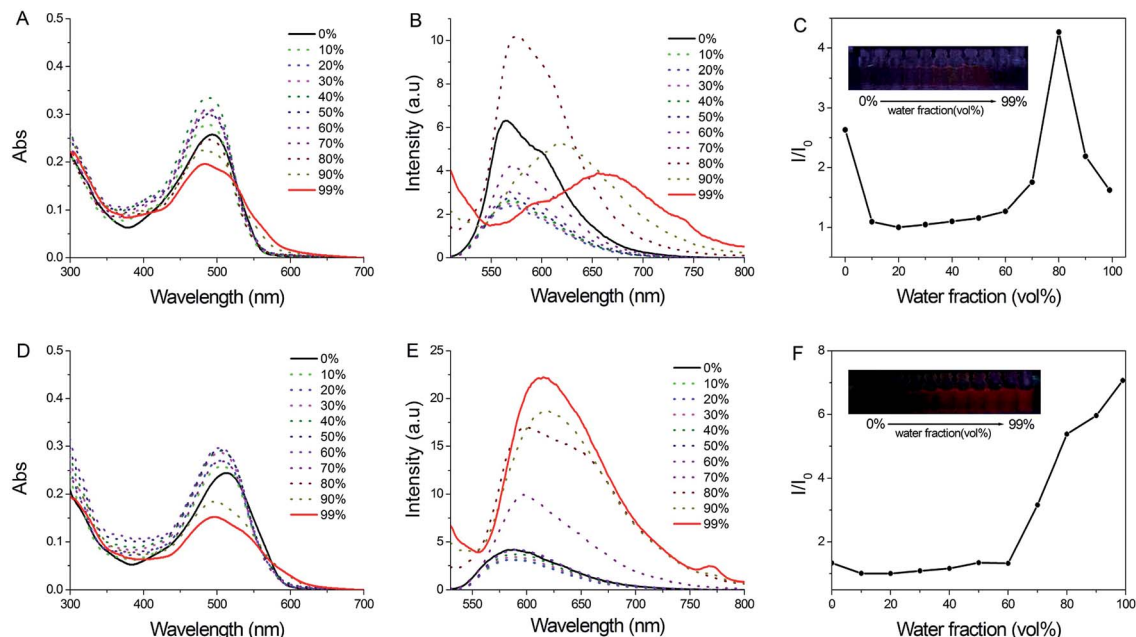
Fig. 2 (A) Absorption, (B) fluorescence and (C) relative fluorescent intensity (I/I_0) change of **PHPO-BF$_2$** in THF/H$_2$O mixed solution with different water fraction; (D) absorption, (E) fluorescence and (F) relative fluorescent intensity (I/I_0) change of **NHPO-BF$_2$** in THF/H$_2$O mixed solution with different water fraction (1.0 × 10^{-5} M; inset: fluorescent images).

the fluorescence intensity always increases with water content increasing. Meanwhile, a slight red shift of fluorescence occurs, and a new shoulder absorption band appeared around 600 nm, manifesting the formation of J-aggregate. Compared to **PHPO-BF$_2$**, no fluorescence quenching was observed during the aggregation even at f_w 99% (Φ_f = 3.1%), possibly due to the formation of comparatively smaller particles with uniform size distribution (Fig. S7†).

In order to understand the AIEE characters of these two boron-difluoride dyes, single crystal of **PHPO-BF$_2$** suitable for X-ray single crystal diffraction was cultivated from a mixed solvent of dichloromethane and petroleum ether. As shown in Fig. 3, the B–N bond distance is measured to be 1.59 Å, and the B–O bond length is 1.46 Å, manifesting the asymmetry of the molecule. The F–B–F group acted as a bifurcated acceptor with an angle of 112.18°. As a fluorescent chromophore, the conjugated BF$_2$ chromophore exhibits good planarity with the mean deviation from the whole π system 0.057 Å (except for the B–F moiety and the phenyl ring). The angle between the chromophore plane and O–B–N plane is estimated to be 31.21°, and the angle between the chromophore plane and the phenyl ring is 47.14°, demonstrating a non-planar molecular conformation (Fig. S8†). Due to the high planarity of the phenanthrene ring, intermolecular π–π interaction between neighbouring phenanthrene rings is present in the crystal structure. In fact, a trimeric "sandwich"-like structure was found. The phenanthrene ring in one **PHPO-BF$_2$** molecule overlaps with the phenanthrene rings in other two neighbouring molecules. It's noteworthy that the π–π overlapping only exists between phenanthrene ring, possibly due to that the phenyl ring is not in the same plane with the chromophore plane. The

intermolecular π–π interactions in molecular clusters were estimated by density functional theory (DFT) calculation using M062x functional (shown as "green cloud" in Fig. 3C). Aided by the π–π stacking between the phenanthrene ring in **PHPO-BF$_2$** molecule, one-dimensional stacking mode was formed. But this one-dimensional stacking has two kinds of different aggregations. Two **PHPO-BF$_2$** molecules in one packing type adopt an antiparallel arrangement with interplanar distance 3.38 Å, and most of the whole phenanthrene ring overlaps with another one, representing H-aggregation. Another two molecules have a longer interplanar distance of 3.42 Å with partial overlapping, indicating J-aggregation.[47] Since the overlapping of the intermolecular π system is partial, the crystal emits visible long-wavelength aggregate emission with quantum yield 3.0% (τ 3.34 ns).
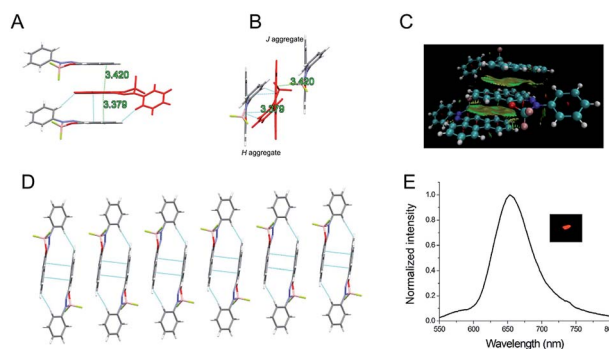

Fig. 3 Single crystal of **PHPO-BF$_2$** (A) side view along *x* axial; (B) side view along *z* axial; (C) intermolecular interactions (shown as green cloud); (D) one-dimensional stacking; (E) fluorescent spectra and image.
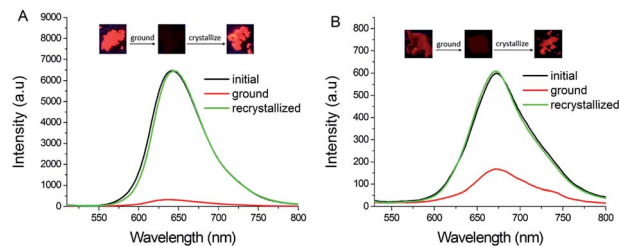
Fig. 4 (A) Fluorescent spectra and images of **PHPO-BF₂** during mechanochromism; (B) fluorescent spectra and images of **NHPO-BF₂** during mechanochromism.

Fig. 6 Information writing and erasing processes.

Considering that **PHPO-BF₂** could form emissive and non-emissive aggregates during the precipitating process in THF, we suppose these boron-difluoride derivatives may be able to exhibit reversible mechanofluorochromism. As shown in Fig. 4, the initial powder of **PHPO-BF₂** emits visible red fluorescence at 642 nm with lifetime 3.46 ns. The fluorescence quantum yield is estimated to be 4.6%. Upon mechanical grinding in a mortar, the fluorescence intensity gradually weakens and turns almost completely quenched and invisible by naked eyes. Crystallization from mixture of dichloromethane and petroleum ether or fume by dichloromethane or heat could recover its fluorescence, manifesting reversible mechanochromism. Similar mechanochromic phenomenon was observed for **NHPO-BF₂**. The initial powder of **NHPO-BF₂** emits intense near-infrared fluorescence at 672 nm (Φ_f: 1.5%, τ: 1.30 ns). The emission of the initial powder was quenched significantly after grinding, and it could be recovered completely by recrystallization.

In order to investigate the mechanochromic mechanism of these two boron-difluoride dyes, all samples were subjected to XRD measurements. The initial solid powder of **PHPO-BF₂** exhibits intense and sharp reflections, demonstrating a crystalline structure (Fig. 5). Notably, the reflections of the initial powder resemble most peaks of the simulated peaks of the single crystal (Fig. S9†), revealing that the initial powder might possess similar molecular packing mode with that in single crystal. After grinding in the mortar, most diffraction peaks disappeared or significantly weakens, suggesting that the ground powder turns amorphous. Currently, it's difficult to understand the molecular packing modes that determined amorphous samples' fluorescence properties. Considering that 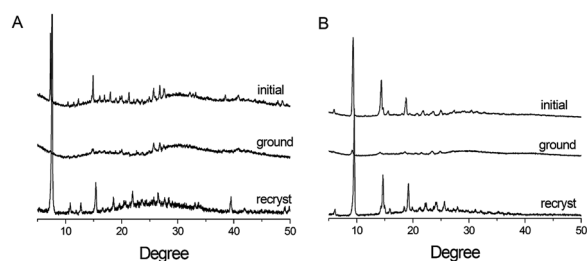the structure of **PHPO-BF₂** optimized by B3LYP with the 6-31+G(d,p) basis sets exhibits better planarity compared to that in single crystal, we suppose the planar structure of **PHPO-BF₂** might facilitate the formation of J-aggregate with more intense intermolecular π–π interactions (shorter interplanar distance and greater overlapping degree), which could quench the fluorescence. The hypothesis is further supported by the potential molecular packing obtained by polymorph prediction, and the intermolecular π–π interactions turn much more intense for the conformation with planar structure (Fig. S10†). Thus, we propose that the grinding might intensify the intermolecular π–π interactions, and the mechanochromic mechanism might be the reversible conversion from emissive H(J)-aggregate with medium intermolecular π–π stacking to non-emissive J-aggregate with intense intermolecular π–π interactions. Similar mechanochromic phenomenon is observed for **NHPO-BF₂**. Therefore, the fluorescence changes of **PHPO-BF₂** and **NHPO-BF₂** upon mechanical force could be ascribed to the stimuli-induced changes of intermolecular π–π interactions.

Since these two AIEE boron-difluoride dyes showed high-contrast mechanochromic properties, they might be adopted for applications in memory field. Here, **PHPO-BF₂** is chosen as an example to demonstrate its application in optical recording. First, a filter paper was immersed in a concentrated solution of **PHPO-BF₂** in chloroform, and then dried. The initial paper emits intense red fluorescence. A black "AIE" stamp could be written on the red background using a stainless steel spatula (Fig. 6). The stamp could be easily erased upon fuming with dichloromethane or heating. And the recovered paper could be used for imputing information again.

4 Conclusions

We synthesized two novel boron-fluoride derivatives, using phenanthrenequinone hydrazone derivatives as ligands. These two dyes emit weak fluorescence in dilute solutions, but enhanced emissions were observed in aggregate state. Owing to the asymmetric structure, these boron-difluorides possess comparatively large stokes shift (over 70 nm). Because the phenyl (naphthyl) ring could rotate to provide planar or non-planar conformations, multiple stacking modes with different intermolecular π–π interactions were found in their aggregate state. The conformation in single crystal structure of **PHPO-BF₂** is non-planar and the intermolecular π–π interaction is medium, making the crystal emit visible red fluorescence. In a planar conformation, intense intermolecular π–π interactions exists to quench the fluorescence, which is supported by polymorph prediction. Grinding might change the conformation of these molecules to intensify the intermolecular interactions, and then quench their fluorescences. Therefore, the

Fig. 5 XRD patterns of **PHPO-BF₂** (A) and **NHPO-BF₂** (B) during mechanochromism.

Paper

mechanochromic mechanism of these boron-difluoride dyes is ascribed to the stacking model transition between H(J)-aggregation formation with loose molecular packing and J-aggregation with intense intermolecular interactions.

Conflicts of interest

There are no conflicts to declare.

Acknowledgements

Notes and references

1 M. Mao, S. Xiao and J. Li., *Tetrahedron*, 2012, **68**, 5037–5041.
2 Y. Deng, Y. Y. Cheng, H. Liu, J. Mack, H. Lu and L. G. Zhu, *Tetrahedron Lett.*, 2014, **55**, 3792–3796.
3 J. F. Araneda, W. E. Piers, B. Heyne, M. Parvez and R. McDonald, *Angew. Chem., Int. Ed.*, 2011, **50**, 12214–12217.
4 H. Liu, H. Lu, J. Xu, Z. P. Liu, Z. F. Li, J. Mack and Z. Shen, *Chem. Commun.*, 2014, **50**, 1074–1076.
5 S. Z. Xiao, Q. Cao and F. J. Dan, *Curr. Org. Chem.*, 2012, **16**, 2970–2981.
6 S. Wang, R. H. Tan, Y. Q. Li, Q. Li and S. Z Xiao, *Dyes Pigm.*, 2016, **132**, 342–346.
7 S. Wang, H. C Lan, S. Z. Xiao, R. H. Tan and Y. X. Lu, *Chem.–Asian J.*, 2017, **12**, 198–202.
8 S. Wang, S. Z Xiao, X. H. Chen, R. H. Zhang, Q. Cao and K. Zou, *Dyes Pigm.*, 2013, **99**, 543–547.
9 X. H. Chen, S. Z. Xiao, S. Wang, Q. Cao, K. Zou, N. Y. Huang and Z. S. Deng, *Tetrahedron Lett.*, 2013, **54**, 4116–4120.
10 Q. Cao, S. Z. Xiao, M. F. Mao, X. H. Chen, S. Wang, L. Li and K. Zou, *J. Organomet. Chem.*, 2012, **717**, 147–151.
11 M. F. Mao, S. Z. Xiao, J. F. Li, Y. Zou, R. H. Zhang, J. R. Pan, F. J. Dan, K. Zou and T. Yi, *Tetrahedron*, 2012, **68**, 5037–5041.
12 H. Liu, H. Lu, Z. K. Zhou, S. Shimizu, Z. F. Li, N. Kobayashi and Z. Shen, *Chem. Commun.*, 2015, **51**, 1713–1716.
13 J. Luo, Z. Xie, J. W. Y. Lam, L. Cheng, H. Chen, C. Qiu, H. S. Kwok, X. Zhan, Y. Liu, D. Zhu and B. Z. Tang, *Chem. Commun.*, 2001, **18**, 1740–1741.
14 Y. P. Qi, Y. T. Wang, G. X. Ge, Z. Y. Liu, Y. J. Yu and M. Xue, *J. Mater. Chem. C*, 2017, **5**, 11030–11038.
15 J. B. Su, W. P. Chen, F. Wu, X. Y. Bai, W. W. Du, L. P. Fang, Y. G. Wu, X. Wen, H. J. Wang and X. W. Ba, *Dyes Pigm.*, 2019, **162**, 808–814.
16 H. Z. Gao, D. F. Xu, Y. H. Wang, X. L. Liu, A. X. Han and C. Zhang, *Dyes Pigm.*, 2018, **150**, 59–66.
17 L. Zhai, F. S. Zhang, J. B. Sun, M. Y. Liu, M. Sun and R. Lu, *Dyes Pigm.*, 2017, **145**, 54–62.
18 K. Suenaga, K. Tanaka and Y. Chujo, *Eur. J. Org. Chem.*, 2017, **35**, 5191–5196.
19 Z. Q. Zhang, Z. Wu, J. B. Sun, P. C. Xue and R. Lu, *RSC Adv.*, 2016, **6**, 43755–43766.
20 D. Wu, L. Shao, Y. Li, Q. L. Hu, F. H. Huang, G. C. Yu and G. P. Tang, *Chem. Commun.*, 2016, **52**, 541–544.
21 Q. S. Liu, X. Q. Wang, H. Yan, Y. P. Wu, Z. Y. Li, S. W. Gong, P. Liu and Z. P. Liu, *J. Mater. Chem. C*, 2015, **3**, 2953–2959.
22 K. Perumal, J. A. Garg, O. Blacque, R. Saiganesh, S. Kabilan, K. Kuppusamy and K. Venkatesan, *Chem.–Asian J.*, 2012, **7**, 2670–2677.
23 Y. Meesala, V. Kavala, H. C. Chang, T. S. Kuo, C. F. Yao and W. Z. Lee, *Dalton Trans.*, 2015, **44**, 1120–1129.
24 S. W. Gong, Q. S. Liu, X. Q. Wang, B. Xia, Z. P. Liu and W. J. He, *Dalton Trans.*, 2015, **44**, 14063–14070.
25 K. I. Lugovik, A. K. Eltyshev, P. O. Suntsova, P. A. Slepukhin, E. Benassi and N. P. Belskaya, *Chem.–Asian J.*, 2018, **2**, 311–324.
26 X. Q. Wang, Y. P. Wu, Q. S. Liu, Z. Y. Li, H. Yan, C. L. Ji, J. C. Duan and Z. P. Liu, *Chem. Commun.*, 2015, **51**, 784–787.
27 R. H. Tan, Q. F. Lin, Y. Wen, S. Z. Xiao, S. Wang, R. H. Zhang and T. Yi, *CrystEngComm*, 2015, **17**, 6674–6680.
28 R. R. Maar and J. B. Gilroy, *J. Mater. Chem. C*, 2016, **4**, 6478–6482.
29 X. L. Zhu, R. Liu, Y. H. Li, H. Huang, Q. Wang, D. F. Wang, X. Zhu, S. S. Liu and H. J. Zhu, *Chem. Commun.*, 2014, **50**, 12951–12954.
30 J. Zheng, F. Huang, Y. J. Li, T. W. Xu, H. Xu, J. H. Jia, Q. Ye and J. R. Gao, *Dyes Pigm.*, 2015, **113**, 502–509.
31 L. Quan, Y. Chen, X. J. Lv and W. F. Fu, *Chem.–Eur. J.*, 2012, **18**, 14599–14604.
32 Y. Yang, X. Su, C. N. Carroll and I. Aprahamian, *Chem. Sci.*, 2012, **3**, 610–613.
33 Y. P. Wu, Z. Y. Li, Q. S. Liu, X. Q. Wang, H. Yan, S. W. Gong, Z. P. Liu and W. J. He, *Org. Biomol. Chem.*, 2015, **13**, 5775–5782.
34 Y. Kubota, S. Tanaka, K. Funabiki and M. Matsui, *Org. Lett.*, 2012, **14**, 4682–4685.
35 R. Yoshii, A. Hirose, K. Tanaka and Y. Chujo, *Chem.–Eur. J.*, 2014, **20**, 8320–8324.
36 P. Choudhury, S. Sarkar and P. K. Das, *Langmuir*, 2018, **34**, 14328–14341.
37 A. S. V. Anand, K. Mahesh and V. Priyanka, *J. Mater. Sci.: Mater. Electron.*, 2018, **29**, 10949–10961.
38 Y. Zhang, J. H. Wang, W. Zheng, T. Chen, Q. X. Tong and D. Li, *J. Mater. Chem. A*, 2014, **2**, 4159–4166.
39 B. K. An, S. K. Kwon, S. D. Jung and S. Y. Park, *J. Am. Chem. Soc.*, 2002, **124**, 14410–14415.
40 Q. Zhao, L. Li, F. Y. Li, M. X. Yu, Z. P. Liu, T. Yi and C. H. Huang, *Chem. Commun.*, 2008, **6**, 685–687.
41 Y. Deng, W. Yuan and Z. Jia, *J. Phys. Chem. B*, 2014, **118**, 14536–14545.
42 *Gaussian 09, Revision D.01*, Gaussian, Inc., Wallingford CT, 2013.
43 *Materials Studio*, Accelrys Software Inc., San Diego, 2013.
44 Y. Zhao and D. G. Truhlar, *Acc. Chem. Res.*, 2008, **41**, 157–167.
45 T. Lu and F. W. Chen, *J. Comput. Chem.*, 2012, **33**, 580–592.
46 X. J. Yan, P. C. Zhu, Y. Li, S. Yuan, H. C. Lan and S. Z. Xiao, *Mater. Today Commun.*, 2019, **20**, 100565.
47 Y. B. Shen, P. Chen, J. X. Liu, J. P. Ding and P. C. Xue, *Dyes Pigm.*, 2018, **150**, 354–362.